JOURNAL OF SOLID STATE CHEMISTRY **141,** 392–403 (1998)
ARTICLE NO. SC987960

Percolation and Modeling of Proton Conduction in Polymer/Brushite Composites

Laurence Tortet, Jean-Raymond Gavarri,[1] Jean Musso, and Geneviève Nihoul

Laboratoire des Matériaux Multiphasés et Interfaces, UPRES 2135, Faculté des Sciences et Techniques, Université de Toulon-Var, BP132, F-83 957 La Garde Cedex, France

and

Andrey K. Sarychev

Scientific Center for Applied Problems in Electrodynamics, Russian Academy of Sciences Izhorskay, 13/19, 127412 Moscow, Russia

Received December 24, 1997; in revised form July 14, 1998; accepted July 19, 1998

Composites have been fabricated by compressing polycrystalline brushite mixed with a polymer powder into pellets to study the surface activities and proton mobilities of acid $CaHPO_4 \cdot 2H_2O$ phosphates (brushite). The electrochemical properties of such composites are studied using complex impedance spectroscopy analyses. Two types of surface proton migrations have been observed by following the water content of the samples. The various proton migrations through these granular materials and the percolation threshold of these currents are interpreted using various modeling approaches. Three models are used and compared: the effective medium approximation (EMA), a model based on the percolation theory, and a semiempirical microstructural electrical model.

Key Words: **Hydrated calcium phosphates; Proton mobility; Electrical complex impedance; Composites; Percolation**

I. INTRODUCTION

The primary aim of this study was to better understand the electrochemical behaviors of composite electrolytes elaborated from powders of the acid phosphate $CaHPO_4 \cdot 2H_2O$ (or brushite) and of an insulating polymer. In our previous experimental works (1, 2), we showed that such composites compacted into pellets could be used as proton conductors in battery devices. We also showed that the presence of a water layer, on the surfaces of brushite grains, involved a certain acid character and was at the origin of the observed proton migrations all over the surfaces. In addition, we have evidenced nonlinear variations of the conductances with the volume fractions of constituents. The origin of surface proton conduction in brushite can be expressed as

$$H_2O \text{ (adsorbed on brushite grain surface)} \Leftrightarrow H^+ \text{ (surface)} + OH^- \text{ (adsorbed)}.$$

A percolation threshold was observed in the case of battery devices Cu/composite/Zn with a strong jump in voltage close to a critical value Φ_c of brushite volume fraction. In fact, this critical composition should be of major interest in applications, because, close to this composition, the composite can behave as an electrical switching material when it is subjected to an external mechanical stress.

To characterize the proton motions in such multiphase systems, electrical complex impedance spectroscopy (ECIS) was carried out on composites fabricated by mixing polycrystalline brushite and a passive polymeric matrix, the poly-phenyl sulfur PPS (3). The main role of such a matrix is to control the migration of ionic currents:

1. At low phosphate concentrations, each grain can be isolated in a neutral environment thus locking out any ionic current through the composite sample as no migration path exists in the solid.

2. At higher concentrations, due to the formation of statistical paths through the granular sample, some percolation of ionic currents can be observed.

3. Finally, the presence of porosity, involved by the elaboration process, plays an additional and prominent role in the final properties.

Thus, the study of such composites could be a mean for characterizing the surface phenomena involved in ionic conductivity and for understanding the ionic migration paths.

In this work, we present three types of modeling that allow us to connect the macroscopic electrical behaviors

[1]To whom correspondence should be addressed.

0022-4596/98 $25.00

with the disordered microstructure of these composites. To better understand the application fields of each modeling, we recall first the main experimental features which condition the migration properties.

II. EXPERIMENTAL RESULTS

II.1. The Constituents

Powdered commercial (Aldrich) brushite and polyphenylene sulfide $[\text{-}C_6H_4S\text{-}]_n$, noted PPS, have been used to prepare the composites. This polymer is insulating and chemically neutral. The granulometry was controlled using a Malvern size meter in a polyphase mode analysis. The analysis allows size determinations in the range 0.3 to 300 μm, and assumes the observable particles to be spherical.

A mean diameter of 15 μm for the brushite powder is obtained. The various sizes ranged from 0.5 to 54 μm, with a maximum of 16.6 μm. The particle diameters of PPS are larger than that of brushite, with a mean diameter of 42 μm.

II.2. The Composites

All the composites are prepared in the same conditions. The manufacturing process is, as usual: (1) grinding then mixing the constituents in well-defined proportions, (2) pressing the powdered mixture in a cylindrical cell under a pressure of 1.6 kbar, and (3) determining the overall density in order to calculate the proportion of residual cavities.

The volume fractions are then calculated using the initial weights of constituents, the individual density of each constituent, and the effective volume of the pellets. The macroscopic properties will be functions of the volume fractions (Φ_{brushite}, Φ_{cavities}, Φ_{PPS}), where

$$\Phi_{\text{brushite}} + \Phi_{\text{cavities}} + \Phi_{\text{PPS}} = 1.$$

The final composite samples are cylindrical pellets (diameter, 20 mm; height, 2 to 5 mm). Both matrix and brushite are powders and for all volume fractions, the composite pellets have a significant proportion of cavities (13% for pure PPS and 27% for brushite). In these cavities, the proton species bound to the adsorbed water can move along the surface of the grains when an electrical field is applied. First investigations (1, 2) have shown that when no adsorbed water was present, no conductivity was observed.

In these previous studies, two series of brushite/PPS composites were prepared. In one case, the preliminary brushite and PPS powders were kept under ambient atmosphere (series I, "dry"), whereas in the second case, these powders were preliminary kept under wet atmosphere (series II, "wet"). Each sample was subjected to electrical complex impedance measurements for frequencies ranging from 10^{-1} to 10^4 Hz.

II.3. Electrical Complex Impedance Spectroscopy (ECIS) $Z[\omega, \Phi]$

The electrical complex impedances $Z[\omega, \Phi]$ were measured from a potentiostat/galvanostat Model 273A from EGG, coupled with a HF frequency response analyzer SI1255 from Schlumberger. Each sample was put between two gold electrodes with a constant pressure, at 25°C. The working frequency ω automatically varies between 10^{-1} and 10^{+4} Hz. The results will be represented either in $(\log|Z|, \Phi)$ graphs or in Nyquist graph ($X = Z'$, $Y = -Z''$), where the complex impedance is $Z = Z' + jZ''$.

Nyquist representations are interesting for us because they clearly show the difference between insulating and conducting states of samples. In addition, they allow a clear separation between bulk and electrode interface contributions. To better represent the paths available for ionic migrations (2), each diagram will be reported as a function of the sum of brushite and cavities volume fractions: $\Phi = \Phi_{\text{Bru}} + \Phi_{\text{cav}}$. This result is recalled in the first paragraph of the modeling, which concerns the effective medium approximation.

For volume fractions lower than 0.25, the composites of series I exhibit a quasi-pure capacitance behavior. For volume fractions higher than the value of 0.3, at least two main contributions are observed: (i) the bulk contribution (represented by the circular part for higher frequencies) corresponding to classical (R,C) circuits and (ii) the electrode surface contribution (represented by the roughly linear region for lower frequencies) due to migration of ionic species at the interfaces. Using the total fraction of phosphate plus cavities, at $\Phi_c = 0.25$, a sharp transition between the insulating and conducting states is clearly observed.

In Fig. 1, some selected Nyquist representations of the series II (wet atmosphere) composites are reported. The critical volume fraction $\Phi_c = 0.24$ is close to the value found in the case of series I.

Nyquist diagrams of a brushite-rich composite ($\phi = 0.4$) and of a pure brushite, in which ionic conduction occurs, are reported in Figs. 1c and 1d. In the case of such high brushite fractions, two circular contributions can be observed: this could be due to two types of mobilities, or to two types of charge carriers (H^+, OH^-, H_3O^+, …).

III. MODELINGS

To interpret the previous ECIS data, three types of modeling are proposed: the effective medium approximation (noted EMA), the percolation theory, and the microstructural approach.

III.1. Effective Medium Approximation (EMA)

The effective medium approximation (EMA) (3–5) can describe the behavior of the transport property Σ mainly

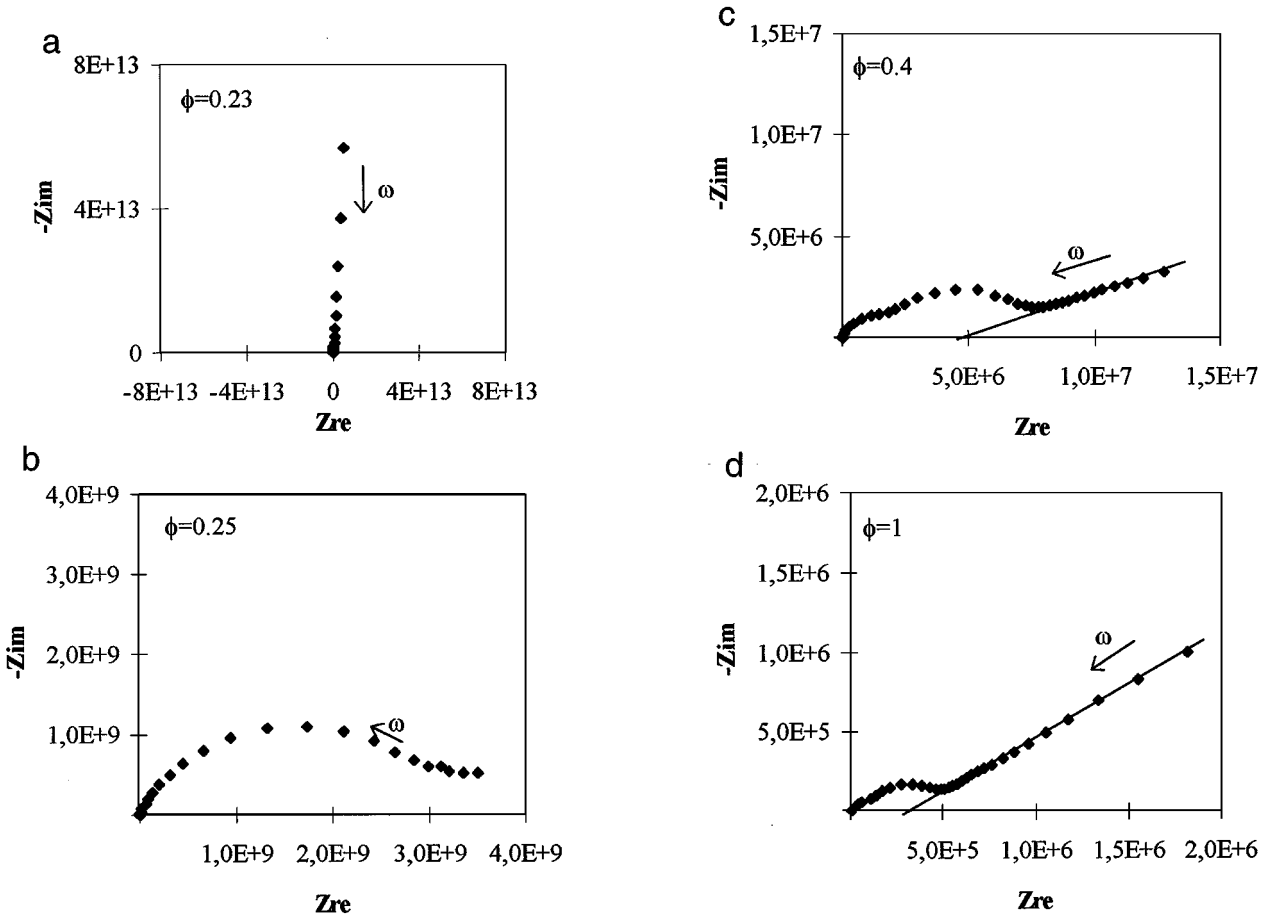

FIG. 1. Nyquist representations of wet Brushite/PPS composites (series II): (a, b) extreme Nyquist graphs at $\Phi < 0.24$, $\Phi > 0.24$, which show the transition between the insulating and the conducting states in the composites Bru/PPS; (c, d) Nyquist diagrams of the composite ($\Phi = 0.4$) and of pure brushite ($\Phi = 1$). The circular part is connected with proton conduction in the electrolyte granular medium. The linear part observed at low frequency is directly connected with the proton reactions and diffusions at the electrodes.

when the composition is sufficiently close to that of the pure constituent (σ_1 and σ_2 for $\phi = 0$ or 1 in volume fraction)

$$[[\Sigma - \sigma_1]/\Sigma_1]\cdot\Phi_1 + [[\Sigma - \sigma_2]/\Sigma_2]\cdot\Phi_2 = 0, \quad [1]$$

where Φ_1 and Φ_2 are the volume fractions of the two constituents with $\Phi_1 + \Phi_2 = 1$.

The complex conductances (admittances) are such that $\Sigma_{1,2} = \sigma_{1,2} + (d-1)\Sigma$, where d is the dimensional parameter (generally $d = 3$ in the case of a 3D connectivity).

For a 3D ($d = 3$) behavior, a critical composition (percolation) can be defined as $\Phi_c = 1/d = 0.33$. At this step, it should be noted that the previous relation does not take into account the role of the interfaces between grains, which is a weak link in our case.

Thus, the behavior of our composites can be modeled using this classical effective medium approximation (EMA), applied to mobile proton species migrating along grain surfaces or through the bulk.

When the data are considered as functions of the sum $\Phi_1 + \Phi_2$ ($= \Phi_{bru} + \Phi_{cav}$), the $d = 3.1$ (± 0.25) value is found (see Fig. 2). It can be concluded that both brushite and cavities should condition the migration. This confirms our previously stated result that most of the conduction is due to displacement of proton species on the surface of brushite grains and in cavities.

In Fig. 3, Nyquist representations are presented to compare the experimental data with the calculated data at $\phi = 0.67$ (Fig. 3a) and 0.4 (Fig. 3b). The agreement is not good near the percolation composition ($\Phi_c = 0.25$). In fact, this discrepancy between the EMA model and our experimental data was also observed in Fig. 2 ($\log|Z|$ variations). The fit is better for $\Phi = 0.67$ as the composition is far from the percolation composition.

III.2. Percolation Theory

The main result of the percolation theory (5–11) resides in the fact that each transport property (conductance) can be

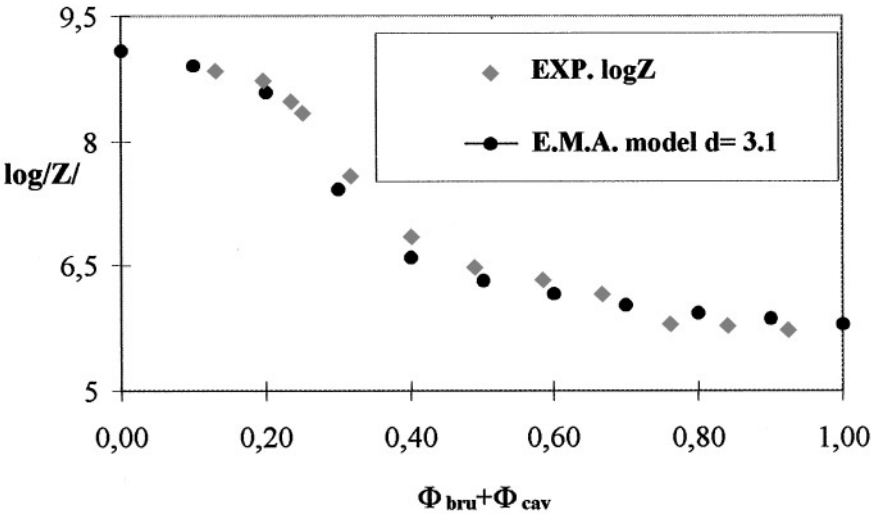

FIG. 2. Superposition of experimental and theoretical ($d = 3.1$) curves of $\log|Z|$ as a function of the sum of volume fractions of brushite and cavities.

developed close to the percolation threshold, Φ_c, as

$$\Sigma = (\Phi - \Phi_c)^t,$$

where t is a critical exponent linked with the formation of infinite conducting clusters through the composite above the Φ_c volume fraction.

The existence of a percolation threshold is observed for the electrical measurements. For a volume fraction of brushite and cavities equal to 0.25, the complex impedance spectroscopy clearly indicates a rapid evolution directly linked with the formation of continuous paths through the composites: along these paths, mobile ionic species migrate when an electrical field is applied between the electrodes.

In the percolation theory, the material impedance can be represented by a simplified equivalent circuit (RC parallel) in a first approximation, as represented in Eq. [2]. The mobile species are susceptible to jumping from site to site, with a residence time τ.

$$Z = \frac{Z_0(\Delta\phi)^{-t}}{1 + (j\omega\tau)^{\alpha}}, \qquad [2]$$

where $\Delta\phi = \phi - \phi_c$, ϕ_c is the critical volume fraction, τ is the residence time of the mobile particle, t is the transport

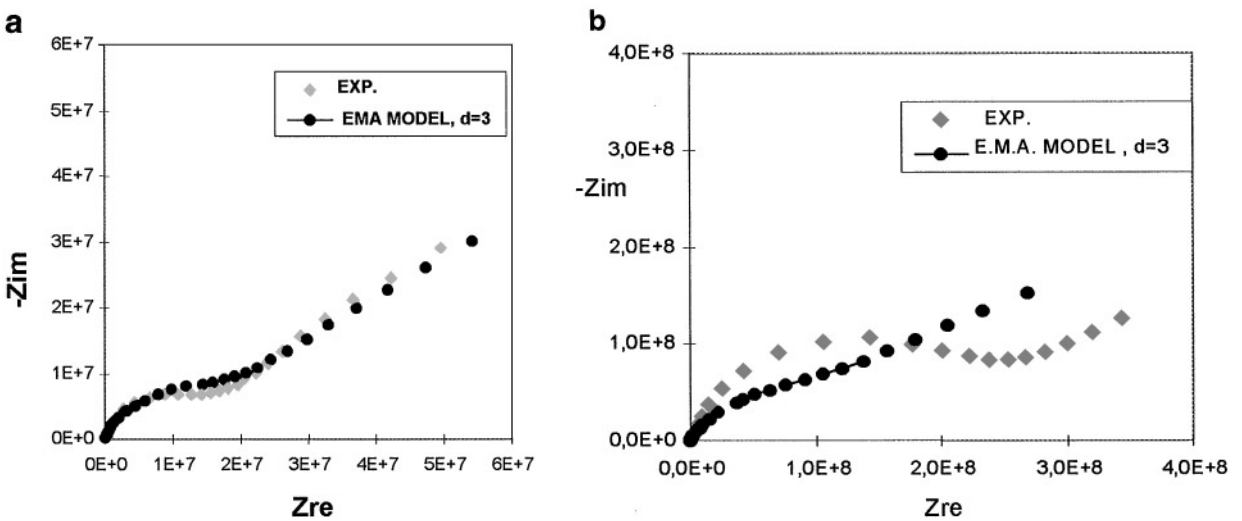

FIG. 3. Superposition of the experimental Nyquist representations (series I) with the theoretical Nyquist representations, obtained using the EMA with $d = 3$; 3a: $\Phi = 0.67$; 3b: $\Phi = 0.40$.

critical exponent, and α represents the distribution of the residence times (or relaxation times) around the mean τ value, induced by the inhomogeneity of the granular composites.

$$Z_0 \text{ is a constant, } R = Z_0(\Delta\phi)^{-t}.$$

A comparison can be made between this equation [2] and the classical equation [3] of the RC model, with $\alpha = 1 - \beta$ and $\tau = RC$;

$$Z = \frac{R}{1 + (jRC\omega)^{(1-\beta)}}, \qquad [3]$$

where R is composite resistance, C is composite capacitance, $\tau = RC = 1/\omega_0$ is the relaxation time of the particle and $(1 - \beta)$ characterizes the distribution of activation energies, and $(\beta = 0)$ represents the ideal Debye relaxation.

The imaginary term

$$(j)^{-\beta} = (\cos(-\beta\pi/2) + j\sin(-\beta\pi/2))$$

allows one to determine the depression angle $-\beta\pi/2$.

III.2.1. Normalized Bulk Contribution to Ionic Conductivity

The surface effects at the electrodes are suppressed in order to consider only the bulk contribution. The Nyquist representation of the wet composite $\phi = \phi_{bru} + \phi_{cav} = 0.4$ (series II) is given as example (see Fig. 1c). The contribution of electrode interfaces (straight line at the low frequencies) is eliminated: $Z_{bulk} = -Z_{im} + Z_{im}^{el}$. Z_{im}^{el} is the imaginary coordinate of the straight line.

In order to normalize the curves, the Z_{re} and $Z_{bulk} = -Z_{im} + Z_{im}^{el}$ values are divided by the resistance R value of the compound $(R = Z_0(\Delta\phi)^{-t})$. On the Nyquist representation, the intersection of the semicircle with the real axis delivers the R value.

These transformations are realized on the two complete series of Brushite/PPS composites. The results for different volume fractions of the series II are superposed on Fig. 4. In the case of the first series, the same results are obtained with only one semi-circle.

III.2.2. Calculations of the Various Parameters from Equations [2] and [3]

If $$Z' = \frac{Z}{Z_0(\Delta\phi)^{-t}} = \frac{1}{1 + (j\omega\tau)^{\alpha}} = \frac{Z}{R},$$

then

$$(Z' - 1)/Z' = -(j\omega\tau)^{\alpha} \quad \text{and} \quad |(Z' - 1)/Z'| = \omega'^{\alpha}$$

$$\log|(Z' - 1)/Z'| = \alpha\log(\omega\tau).$$

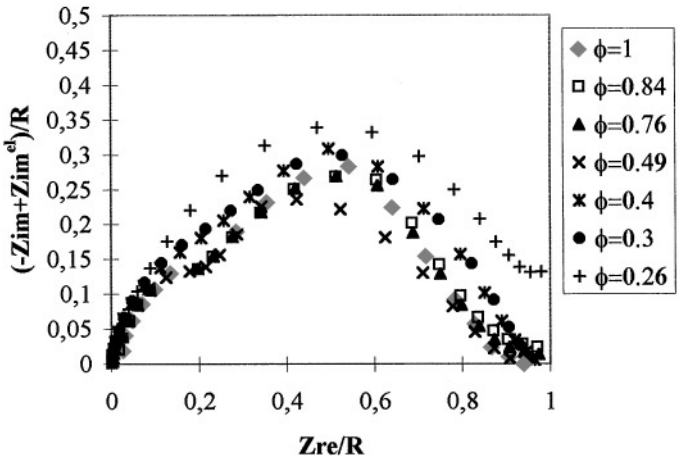

FIG. 4. Superposition of the curves $[(-Z_{im} + Z_{im}^{el})/R;\ Z_{re}/R]$ for different compositions of the (wet) series II.

α and τ can be calculated with the curve $\log|(Z' - 1)/Z'|$, or

$$\log\sqrt{\frac{(Z_{re} - 1)^2 + Z_{im}^2}{Z_{re}^2 + Z_{im}^2}},$$

as a function of $\log\omega$. Z_{re} and Z_{im} are the results of the last normalization, i.e., Z_{re}/R and $(-Z_{im} + Z_{im}^{el})/R)$, respectively. The results are shown in Fig. 5 (series I, Fig. 5a; series II, Fig. 5b).

In the case of series I, the curves are all straight lines. In series II (wet), the curves present two straight lines separated by an inflection zone. These two different sections correspond to the two Nyquist semicircles.

The slope of these curves give the α values, and their extrapolations, when $\log\omega = 0$, permit one to calculate the residence times τ. The obtained results are presented in Table 1 (series I) and in Tables 2 and 3 (series II), and are directly compared with the results obtained using Eq. [3]. $(1 - \beta)$ and τ are directly calculated from the Nyquist representations; the intersection of the circle with the real axis delivers the R value and the maximum of the imaginary part $(-Z_{im})$ corresponds to the frequency $\omega_0 = 1/RC = 1/\tau$. The $-\beta\pi/2$ term is the depression angle of the circle with the real axis (Z_{re}).

A good agreement is observed between the results obtained from the percolation theory and from the classical RC model. They can give some information on the particle behavior in the composites. The ionic mobilities, which appear in series I and II at the medium frequencies, seem to be similar. In the two cases, the medium α value is 0.8; this means that in percolation theory the particle motion is not an ideal diffusion, but corresponds to jumps from site to site with a nonnegligible residence time on sites.

The residence times of series II are weaker; a more important rate of adsorbed water is present in the composites.

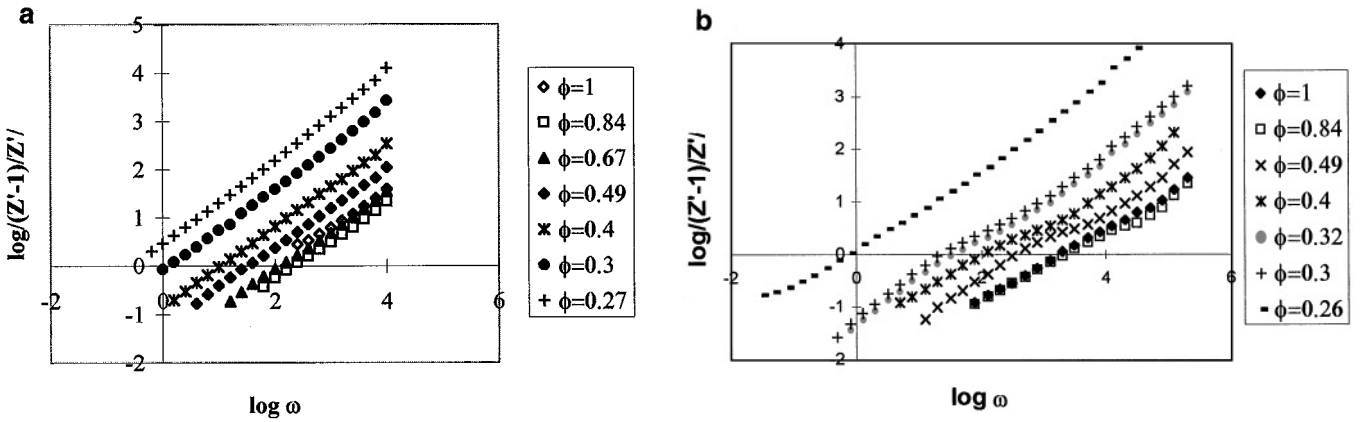

FIG. 5. Superposition of the curves $\log|(Z'-1)/Z'|$ as functions of $\log\omega$ (in Hz), in the case of different compositions in volume fraction $\phi = \phi_{bru} + \phi_{cav}$, in the case of (a) series I and of (b) series II.

Another type of motion appears at high frequencies in series II; $\bar{\alpha} \approx 0.98 \approx 1$ is characteristic of a free diffusion.

III.2.3. Calculation of the Percolation Parameters

According to the percolation theory, Z depends on $\Delta\Phi$ and ω:

$$Z(\Delta\Phi, \omega) = \frac{Z_0(\Delta\Phi)^{-t}}{1 + (j\omega\tau)^{\alpha}}.$$

Percolation of residence time τ. The residence time $\tau = RC = 1/\omega_0$ characteristic of particle jumps might also be expressed as a function of $\Delta\Phi$ and of another exponent noted a,

$$\tau \approx \tau_0\ \Delta\Phi^{-a},$$

in which τ_0 is a constant.

Then, the a value can be obtained with the slope of the line: $\log\tau = f(\log\Delta\Phi)$. With our experimental data and $\Phi_c = 0.25$, we effectively obtain the lines shown in Figs. 6a (series I) and 6b (series II). If the model is correct, $a = 1.8 \pm 0.2$, and $\tau = \tau_0(\Delta\Phi)^{-1.8}$.

We can then consider

$$Y = \log|(Z'-1)/Z'| = X + A$$

$$= \alpha\log\omega + \alpha\log\tau = \alpha[\log\omega + \log\tau_0] - \alpha a\log\Delta\Phi$$

$$X = \alpha[\log\omega - a\log\Delta\Phi]$$

$$A = \alpha\log\tau_0.$$

If we represent the experimental Y values as a function of X, all the points collapse on a single curve.

Percolation of the conduction term R. The t exponent is a universal percolation parameter. It is theoretically equal to 1.9 in the three dimensional (3D) case (5).

TABLE 1
Parameters Related to Eqs. [2] and [3] in the Case of Series I

	Percolation model		*RC* model	
$\phi_{bru} + \phi_{cav}$	α	τ (s)	$1-\beta$	τ (s)
0.27	0.89	3.1	0.84	3.5
0.30	0.86	0.7	0.86	0.7
0.4	0.84	0.1	0.84	0.1
0.49	0.81	0.03	0.83	0.03
0.67	0.79	7×10^{-3}	0.80	8×10^{-3}
0.84	0.78	4×10^{-3}	0.78	5×10^{-3}
1	0.76	1×10^{-2}	0.64	2×10^{-3}

Note. $\bar{\alpha} \approx 0.8$.

TABLE 2
Parameters Related to Eqs. [2] and [3] in the Case of Series II, at Medium Frequencies

	Percolation model		*RC* model	
$\phi_{bru} + \phi_{cav}$	α	τ (s)	$1-\beta$	τ (s)
0.26	0.79	1.5	0.77	1.4
0.3	0.92	0.05	0.81	0.04
0.32	0.91	0.04	0.82	0.03
0.4	0.82	6×10^{-3}	0.80	6×10^{-3}
0.49	0.82	3×10^{-3}	0.79	3×10^{-3}
0.76	0.68	5×10^{-4}	0.80	3×10^{-4}
0.84	0.67	5×10^{-4}	0.72	5×10^{-4}
1	0.67	5×10^{-4}	0.73	6×10^{-4}

Note. $\bar{\alpha} \approx 0.8$.

TABLE 3
Parameters Related to Eqs. [2] and [3] in the Case of Series II at High Frequencies

	Percolation model		*RC* model	
$\phi_{bru} + \phi_{cav}$	α	τ (*s*)	$1 - \beta$	τ (*s*)
0.26				
0.3	0.97		0.79	6×10^{-3}
0.32	0.98	7×10^{-5}	0.80	3×10^{-3}
0.4	1	1×10^{-5}	0.84	4×10^{-4}
0.49	0.99	6×10^{-6}	0.84	1×10^{-4}
0.76	0.97	2×10^{-6}	0.88	5×10^{-5}
0.84	0.95	1×10^{-6}	0.83	5×10^{-5}
1	0.95	1×10^{-6}	0.74	

Note. $\bar{\alpha} \approx 0.98$.

We must try to obtain an estimation of t using our ECIS experimental results. Indeed, the percolation equation is

$$Z = \frac{Z_0(\Delta\Phi)^{-t}}{1 + (j\omega\tau)^{\alpha}} = \frac{R}{1 + (j\omega\tau)^{\alpha}}.$$

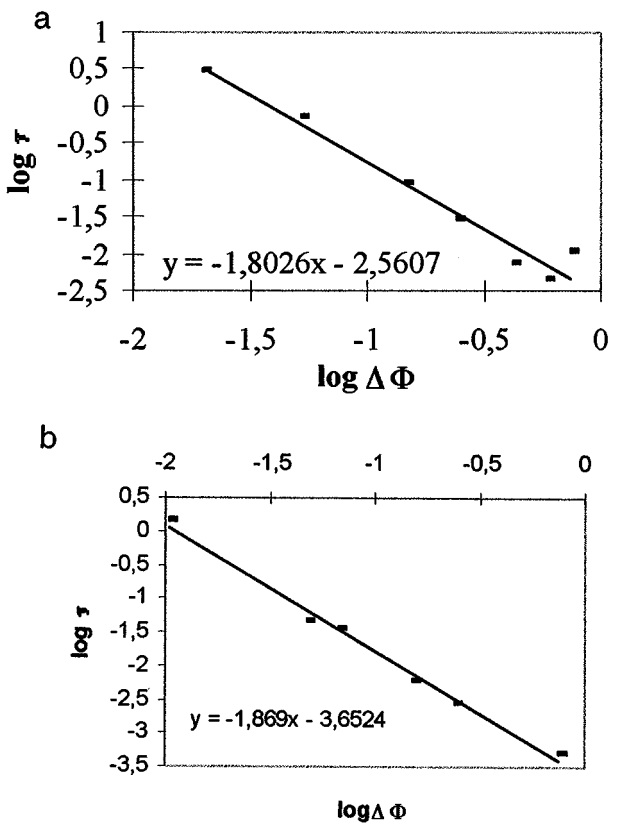

FIG. 6. Representation of the logarithm of τ as a function of $\log\Delta\Phi$ ((a) series I, (b) series II, at medium frequencies).

TABLE 4
Calculation of *t* at Different Frequencies

Frequency (Hz)	10^3	4×10^2	25	10	1	0.251
t (series I)	2.1	2.1	2.1	2.1	1.9	1.8
Frequency (Hz)	1.26×10^4	5×10^2	5	0.2		
t (series II)	0.7	2.2	2.2	0.6		

Note. Series I, t [10 to 10^3 Hz] $= 2.1 \pm 0.2$; Series II, t [5 to 5×10^2 Hz] $= 2.2 \pm 0.2$.

Two approaches have been performed. The first is obtained at a fixed frequency:

$$Z[1 + (j\omega\tau)^{\alpha}] = Z_0(\Delta\Phi)^{-t}.$$

The t value can be obtained with the slope of the curve

$$\log(Z[1 + (j\omega\tau)^{\alpha}] = f(\log(\Delta\Phi)^{-t}) = -t\log\Delta\Phi - t\log Z_0.$$

The calculation of t at different frequencies is done for the two series and reported in Table 4, corresponding to series I and series II.

In the frequency range 10–10^3 Hz, representative of the sample bulk, the obtained t values are 2.1 with series I and 2.2 with series II. The impedance evolution as a function of the frequency is not the same for the two series. For this reason, it is difficult to directly compare their respective results.

In the case of series II, the t value decreases at low and high frequencies. We have not interpreted these results but we suppose that:

— the very high frequencies correspond to the second semicircle; i.e., to the proton free diffusion

— at low frequency ($\omega < 1$ Hz), the electrode/sample interface contribution, which has been subtracted from our experimental data, perturbs the bulk response at intermediate frequency ($1 < \omega < 10^2$ Hz).

A second evaluation of t can be obtained by plotting $\log R$ versus $\log\Delta\Phi$. This is shown in Figs. 7a and 7b. We obtain $t = 2.0$ for series I and $t = 2.2$ for series II.

The main result obtained in this section is the experimental determination of the critical exponents t and a; surprisingly, the t values obtained from our data are in good agreement with the theoretical Monte Carlo calculations found in the literature for "ideal electrical nets".

III.3. Microstructural Electrical Model: Interface Evolutions

An electrical model, previously described in our works (12–16), is first recalled, then used to interpret the proton surface conduction in the present composites, at ambient temperature.

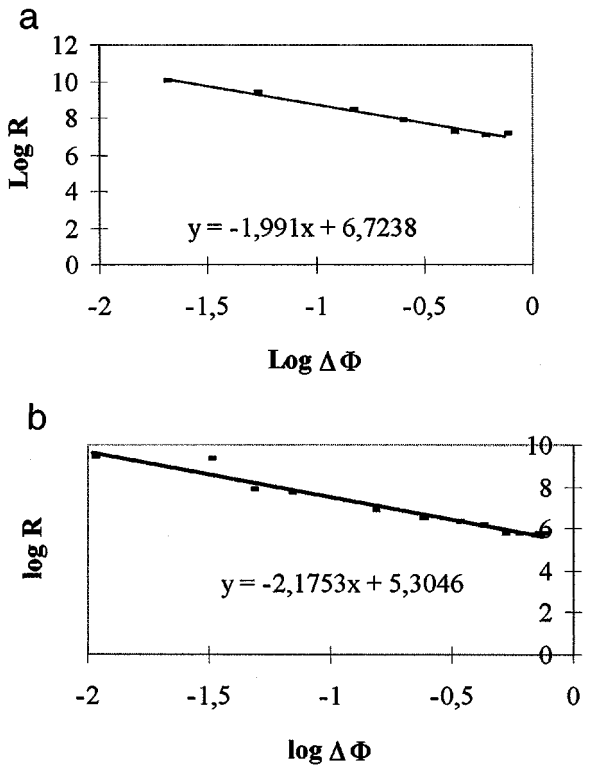

FIG. 7. Representation of the logarithm of R as a function of $\log \Delta\phi$, in the case of (a) series I and (b) series II.

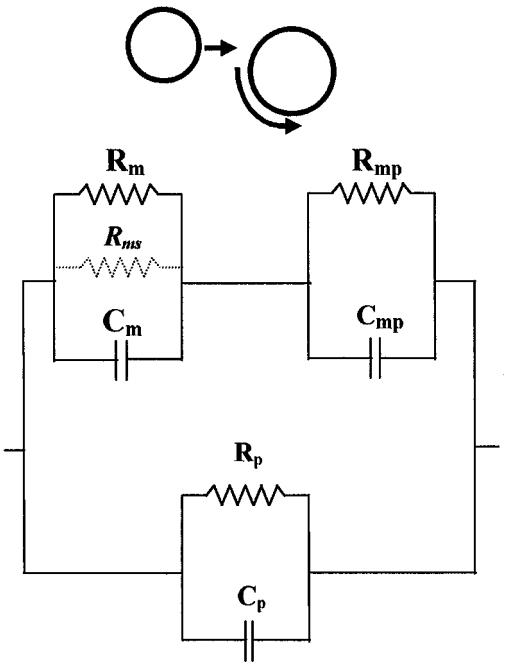

FIG. 8. Equivalent circuit in the case of multiphase material. The subscripts m, p, and mix are, respectively, associated with mineral, polymeric, and intermediate areas.

In this model, the distribution of cubic particles having various sizes was assumed to be regular: it is possible to define the mineral linear fraction $X = (\Phi)^{1/3}$, where Φ is the volume fraction. The alternate zones of mineral crystals and polymer host are represented as electrical complex impedance (resistance R, capacitance C). The resistor–capacitor behavior of the composites can be represented by the general electrical circuit in Fig. 8.

The (RC) equivalent circuits of the various components are noted as follows:

- subscript m for the conducting mineral grains (surface grain conduction),
- subscript p for the polymeric grains (initial matrix areas),
- subscript mp for intermediate zones which are assumed to be due to the formation of bridges between the grains. The conducting properties of this zone are assumed to strongly vary as the volume fraction increases above the percolation composition,
- subscript ms; in the initial model, there is an additional resistance, R_{ms}, which accounts for the *surface* conductivity of the mineral grains. In the present study, where the conductivity still takes place at the grain surface, we have used this resistance to account for the difference between series I and series II; in series I there is only one circle on the Nyquist plot, which means only one RC circuit. R_{ms} will be taken as very weak for this series. For series II, the two circles correspond to the two RC circuit. R_{ms} will be taken higher for this series.

Since we are not interested in the phenomena at the interface sample/electrodes, they are not taken into account in this model; only the high frequency results will be fitted.

The C_m, C_p, and C_{mp} capacitances can play an important role in the case of insulator states (mineral or polymer). The Z_m and Z_p impedance contributions depend on the Φ volume fraction of the mineral. The global impedance $Z(\omega, \phi)$ is a function of ω and Φ,

$$1/Z = \Sigma = 1/Z_p + 1/(Z_m + Z_{mp}). \qquad [4a]$$

In fact, it is necessary to note that the Z_{mp} function must be associated with a third "virtual intermediate phase," which should have its own volume fraction and should be characterized by a "mixed" property. We have represented such a "mixed" intermediate property by "virtual" elemental components noted below R_{mix} and C_{mix}. These two components depend on Φ. Thus, the Z_{mp} term depends on the linear fraction $X = (\Phi)^{1/3}$ and of the terms R_{mix} and C_{mix} (which are also Φ dependent).

Thus, each Z_i impedance (i = p, m, mp) can be expressed as

$$1/Z_m = [1/R_m + jC_m \cdot \omega + 1/R_{ms}]X \qquad [4b]$$

$$1/Z_{mp} = [1/R_{mix} + jC_{mix} \cdot \omega]\ X^2/(1 - X) \qquad [4c]$$

$$1/Z_p = [1/R_p + jC_p\omega]\ (1 - X^2), \qquad [4d]$$

where $X = (\Phi)^{1/3}$ is the linear fraction of the mineral.

This model takes into account the percolation effects; it assumes that the mineral grains are regularly distributed in a continuous matrix which can envelop each grain for low volume fractions of mineral. We recall briefly the semi-empirical approach to describe the percolation.

(1) In some regions between the mineral grains, a percolation distance between them is assumed to exist; the associated percolation is denoted Φ_c, which can be adjusted in order to optimize the experimental data fit.

(2) Due to the presence of variable grain sizes dispersed through the polymeric host, the (RC) values of the polymer between the mineral grains are assumed to be a function of the volume fraction Φ. The more the fraction Φ increases, the more the mineral behavior is prominent. An empirical function (see Ref. (12)) was postulated to account for R_{mix}:

- for $0 < \Phi < \Phi_c$ the evolution is described by

$$R_{mix} = R_p \exp(-A\Phi^2),$$

i.e., for $\Phi = 0$, $R_{mix} = R_p$;

- for $\Phi > \Phi_c$ the evolution is

$$R_{mix} = R_{mix}(\Phi_c) \exp(-B(\Phi - \Phi_c)),$$

with $R_{mix} = R_m$ for $\phi = 1$.

Then, other limit conditions can be proposed. The values of the derivatives of the functions chosen for $\Phi < \Phi_c$ and $\Phi > \Phi_c$ should be equal for $\Phi = \Phi_c$. From these relations the A and B parameters can be calculated as functions of Φ_c. They express the progressive percolation effect due to the distribution of grains.

In the case of series I, the proton mobilities (proton jumps from site to site) at the surface of the grains and between the grains cannot be differentiated, only one semicircle appears on the experimental Nyquist representations. The surface resistance and the intergrain resistance are of the same order of magnitude; the electrical responses overlay.

To fit such a unique proton migration, we have eliminated the Z_m electrical component by creating a short circuit with $R_{ms} = 0\ \Omega$.

To define the Z_{mp} component (with the R_{mix} and C_{mix} virtual components) we have introduced the individual values of Φ_c, R_m, C_m, R_p, C_p,

$$\Phi_c = 0.25,\ R_{ms} = 0\ \Omega,\ R_m = 10^7\ \Omega,\ C_m = 2 \times 10^{-10}\ \text{F},$$

$$R_p = 1 \times 10^{15}\ \Omega,\ C_p = 1 \times 10^{-10}\ \text{F}.$$

The experimental results are reported in Fig. 14, and the theoretical results are reported in Fig. 15.

In the case of series II, we must consider two types of proton migration paths: the first corresponds with proton motions around the grains and the second corresponds with a migration between the grains.

To obtain a good fit of our experimental results at 298 K and in the range $0.01 < \Phi < 0.99$, we have considered both

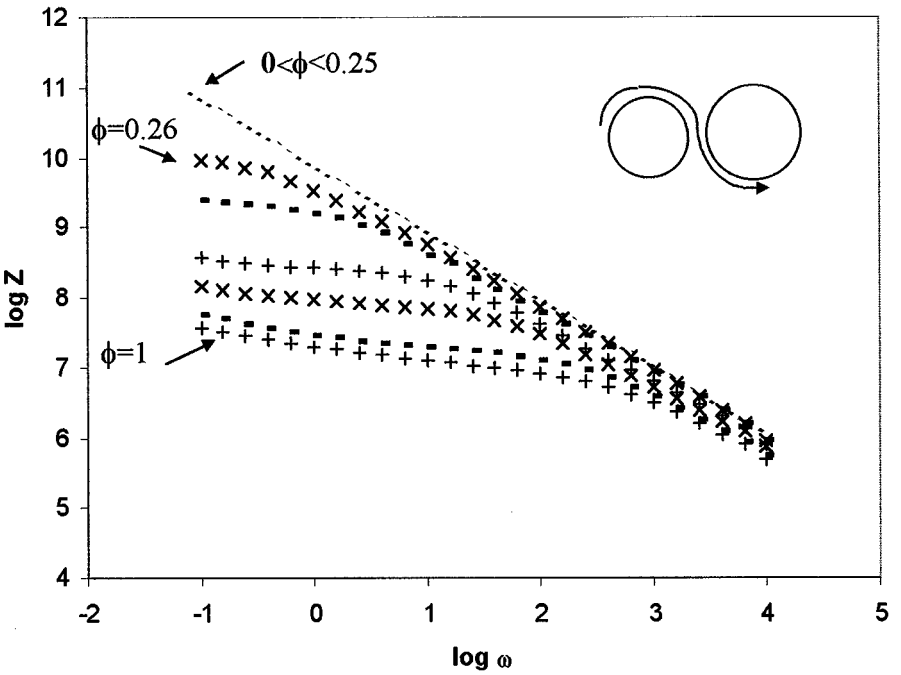

FIG. 9. Representation of $\log|Z|$ as a function of the frequency ω, experimentally obtained for different volume fractions of brushite in PPS (series I). The inset represents the unique continuous path for proton jumps on surface sites.

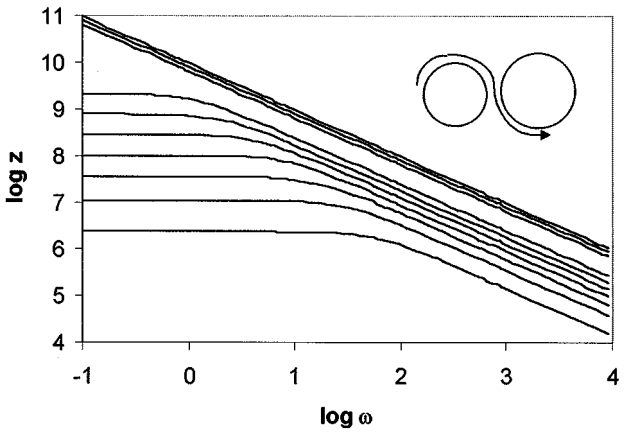

FIG. 10. Microstructural model. Representation of simulated values of $\log|Z|$ as a function of the frequency ω for different volume fractions of brushite in PPS (series I). Note that only one semicircle appears on the corresponding Nyquist representations. The inset represents the unique continuous path for proton jumps on surface sites.

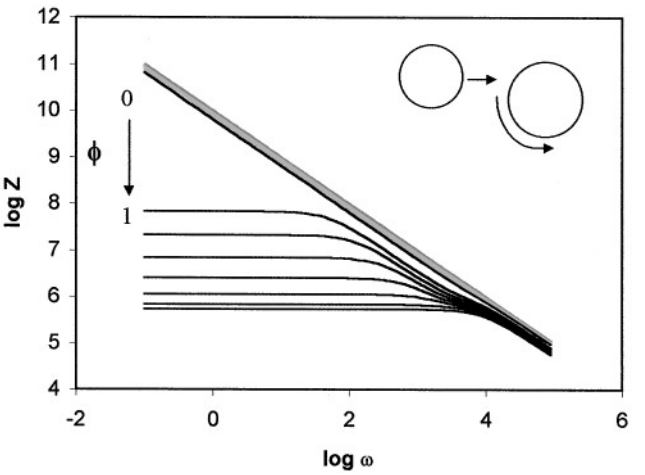

FIG. 12. Microstructural model. Representation of the simulated values of $\log Z$ as a function of the frequency ω for different volume fractions of brushite in PPS (series II).

Z_m and Z_{mp} electrical components using the following hypotheses:

- $\Phi_c = 0.25$;
- the proton conduction around the individual largest grains is associated with $R_m = 5 \times 10^5\ \Omega$, $C_m = 2 \times 10^{-10}$ F, and $R_{ms} = 10^9\ \Omega$ (here, it can be noted that the conduction over the grain surface is conditioned by both R_{ms} and R_m terms and that the conduction for series II is faster than the conduction for series I because of the additional liquid layer);

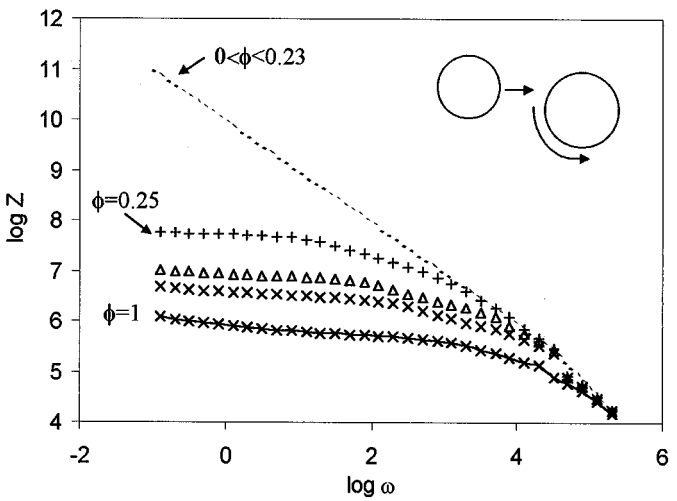

FIG. 11. Representation of $\log Z$ as function of the frequency ω, experimentally obtained for different volume fractions of brushite in PPS (series II). The inset recalls the two types of proton migrations: along one grain surface and between two grains (liquid interface).

- the proton conduction in the "intermediate areas," which condition the percolation behaviors, is represented by the terms R_{mp} and C_{mp}, as given above;
- the polymer contribution is represented by $R_p = 1 \times 10^{15}\ \Omega$, $C_p = 1 \times 10^{-10}$ F.

The little discrepancy between the calculated and experimental curves can be due to the fact that, in our modeling, we have not taken into account the low frequency contributions due to electrode reactions.

Despite these approximations, the impedance values obtained in our model are consistent with our experimental data. The calculated term Z_m delivers a good representation of the impedance around the brushite grains (with the individual components R_m and R_{ms}) in the adsorbed water layer, whereas the term Z_{mp} represents the intermediate medium between the largest grains and allows one to simulate the percolation behaviors above and below Φ_c.

In Fig. 13, two semicircles appear on the experimental and theoretical Nyquist representations.

The main interest of such an approach is to simulate a macroscopic mechanism using individual characteristics of elemental components (surface and interface migrations) and to determine parameters directly linked with a specific microstructure and a specific elaboration process.

IV. DISCUSSION AND CONCLUSION

In the case of our composites presenting interfaces or cavities, we have shown that the proton migrations can be modeled by making use of three different approaches.

In Table 5, we can compare the three modeled expressions of the admittance Σ as a function of the composition parameter Φ: the variation laws are fully different. In fact,

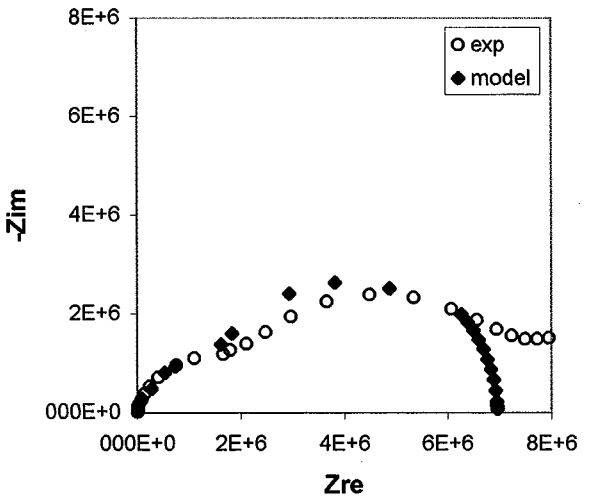

FIG. 13. Superposition of the experimental and theoretical Nyquist representations in the case of the sample ($\Phi = 0.4$) of series II.

they can be used in the case of three different applications: (i) in order to express a global nonlinear evolution for the full composition range when interfaces play a minor role, (ii) to determine the behaviors close to the percolation threshold in the case of electrochemical applications for instance, and, finally, (iii) to express the role of interfaces in the observed conduction.

For our composites, it can be noted that the EMA approach is not satisfactory close to Φ_c because the two-phase model does not take into account the formation of these new interfaces and, as a major fact, it does not consider the statistical existence of any infinite clusters.

The percolation theory, which takes into account the statistical formation of conducting clusters close to the percolation composition, fits very well the results above Φ_c. For the first time, we have applied it to the migration of protons in a mineral/polymer composite. We have found that the critical exponent "$t = 2$" is well associated with a three-dimensional percolation predicted from Monte Carlo calculations. However, this approach also needs the *a priori* knowledge of critical exponents, which depend on the connectivity and the microstructure.

Finally, the microstructural approach which uses many fitting parameters and assumes that the percolation function is well known can be helpful in characterizing the grain interfaces and surfaces. In the case of brushite composites, this approach has given interesting parameters (R_m, C_m, R_{ms}, R_p, C_p), allowing one to characterize the existence of, at least, two types of proton mobilities:

(1) jumps of linked protons H^+ in the adsorbed water near the brushite surface in series I and between the grains in the case of series I and II: the driving parameters are those conditioning the jumps of protons between grains (R_m and C_m).

(2) jumps of free protons H^+ in the quasi-liquid layer of adsorbed water at the brushite surface (in the case of very wet samples): the driving parameters are those linked to the surface of grains (R_{ms}) and to the areas between grains (R_m and C_m).

Now, a new unified approach is needed to improve the description of the electrical responses in disordered granular composites; it should be quite interesting to develop a multiphase percolation model by making use of calculated critical exponents, but also by taking into account the textures and the interfaces between grains. Finally, it should also be quite interesting to take into account the low frequency contributions to improve the simulations of the impedance measurements. The influence of the electrodes must be modeled; this is now in progress and will be presented in another paper.

TABLE 5
The Various Modeled $\Sigma = 1/Z$ Functions for Brushite/Polymer Composites

Type of simulation, conclusions	Admittance (conductance): $\Sigma(\Phi, \omega, T)$
Microstructural approach, identification of surface and intergranular conductions of protons	$\Sigma = 1/Z_p + 1/(Z_m + Z_{mp})$ $R_{mix} = R_p \exp(-A\Phi^2)$ $R_{mix} = R_{mix}(\Phi_c) \exp(-B(\Phi - \Phi_c))$
EMA, global evolution, no agreement close to the percolation composition	$[[\Sigma - \sigma_1]/\Sigma_1] \cdot \Phi +$ $+ [[\Sigma - \sigma_2]/\Sigma_2] \cdot (1 - \Phi) = 0$ $\Sigma_{1,2} = \sigma_{1,2} + (d-1)\Sigma$
Percolation, good agreement close and above the percolation threshold	$\Sigma = (1 + (j\omega\tau_0(\Delta\Phi)^{-a})^z) \cdot \Sigma_0 \cdot (\Delta\Phi)^{+t}$

REFERENCES

1. L. Tortet, J. R. Gavarri, G. Nihoul, J. M. Fulconis, and F. Rouquerol, *Eur. J. Solid State Inorg. Chem.* **33,** 1199 (1996).
2. L. Tortet, J. R. Gavarri, and G. Nihoul, *J. Solid State Ionics* **89,** 99 (1996).
3. L. Tortet, J. R. Gavarri, G. Nihoul, and A. J. Dianoux, *J. Solid State Chem.* **97,** 253 (1997).
4. S. Kirkpatrick, *Rev. Mod. Phys.* **45,** 574 (1973).
5. J. P. Clerc, G. Giraud, J. M. Laugier, and J. M. Luck, *Adv. Phys.* **39,** 3, 191 (1990).
6. J. M. Laugier, J. P. Clerc, and G. Giraud, *in* "Proceedings of International AMSE Conference" (G. Mesnard, Ed.), Lyon, AMSE, 1986.
7. Yi. Song, Won. Noh Tae, Ik. Leesung, and J. R. Gaines, *Phys. Rev. B* **33,** 904 (1986).
8. F. Brouers and A. Ramsamugh, *J. Phys. C* **211,** 839 (1988).
9. D. Stauffer, *Phys. Rep.*, 543 (1979).
10. J. W. Essam, *Rep. Prog. Phys.* **43,** 833 (1980).

11. D. Stauffer, "Introduction to Percolation Theory," Taylor & Francis, London, 1985.
12. C. Alfred-Duplan, J. Musso, J. R. Gavarri, and C. Césari, *J. Solid State Chem.* **110,** 6 (1993).
13. A. Benlhachemi, J. Musso, J. R. Gavarri, C. Alfred-Duplan, and J. Marfaing, *Phys. C* **230,** 246 (1994).
14. A. Benlhachemi, J. R. Gavarri, Y. Massiani, and S. Aïtyazza, *Physica C* **235–240,** 1511 (1994).
15. A. Benlhachemi, J. R. Gavarri, Y. Massiani, and J. Marfaing, *Ann. Chim. Sci. Matériaux* **20,** 335 (1995).
16. C. Alfred-Duplan, J. Marfaing, G. Vacquier, A. Benlhachemi, J. Musso, and J. R. Gavarri, *Mater. Sci. Eng. B* **29,** 1 (1996).